

# Bismuth in strong magnetic fields: unconventional Zeeman coupling and correlation effects

Jason Alicea<sup>1</sup> and Leon Balents<sup>2</sup>

<sup>1</sup>Department of Physics, California Institute of Technology, Pasadena, CA 91125

<sup>2</sup>Kavli Institute for Theoretical Physics, University of California, Santa Barbara, CA 93106-9530

(Dated: October 30, 2018)

Recent experiments on bismuth have uncovered remarkably rich magnetization structure at fields well beyond the regime in which all carriers are expected to reside in the lowest Landau level. Motivated by these findings, we start from a microscopic tight-binding model and derive a low-energy Hamiltonian for the holes and three Dirac electrons pockets in bismuth. We find that an unconventional electron Zeeman effect, overlooked previously, suppresses the quantum limit for the electrons dramatically, giving rise to the observed anomalous magnetization structure. We further study interaction effects near fields at which the 2nd Landau level for one electron pocket empties, where magnetization hysteresis was observed. Here we find instabilities towards both charge density wave and Wigner crystal phases, and propose that hysteresis arises from a first-order transition out of the latter.

PACS numbers:

*Introduction.* After more than a century of active research, bismuth continues to yield fascinating discoveries. Much of this material's exceptional behavior stems from its band structure [1]—the Fermi surface arises from a hole pocket and three Dirac electron pockets which contribute an extremely low carrier density of  $3 \times 10^{18} \text{cm}^{-3}$ . One remarkable consequence of the small carrier concentration is that weak Sb doping is believed to change the system from a semimetal to a topological insulator [2, 3]. Another is that the quantum limit, at which carriers are confined to the lowest Landau level (LLL), can be realized with laboratory fields. In particular, for fields along the highest-symmetry ‘trigonal’ axis, the hole quantum limit occurs at  $\sim 9\text{T}$  [4]. The electron quantum limit, while less clear experimentally, is believed to occur at similar fields [5].

From a single-particle perspective, quantum oscillations should subside once all carriers reside in the LLL, and transport and thermodynamic quantities should appear ‘featureless’. Recent experiments on bismuth in trigonal fields nevertheless observed surprisingly rich physics extending well beyond 9T. Nernst peaks were resolved at 13.3, 22.3, and 30.8T, with the Hall resistance exhibiting step-like features in between, prompting the suggestion that fractionalization may be occurring in this 3D system [6]. More recent torque magnetometry studies at fields near the trigonal axis additionally measured unanticipated magnetization structure—including hysteresis—persisting up to the largest fields probed (31T), providing further evidence for correlation physics [5].

Here we derive a low-energy theory for bismuth, suitable for analyzing the Landau level (LL) structure and interaction effects. For the electrons, we show that strong spin-orbit coupling generates unconventional Zeeman terms not present in the standard Cohen-Blount model [7]. This coupling suppresses the electron quantum limit far beyond 9T for trigonal fields contrary to what has been assumed, recovering the high-field magnetization structure observed in Ref. 5 [see Fig. 1(a)]. Turning to Coulomb effects, we show that interactions have the strongest influence near fields for which a low LL empties. In agreement with this expectation, the experimentally observed hysteresis coincides with one electron pocket

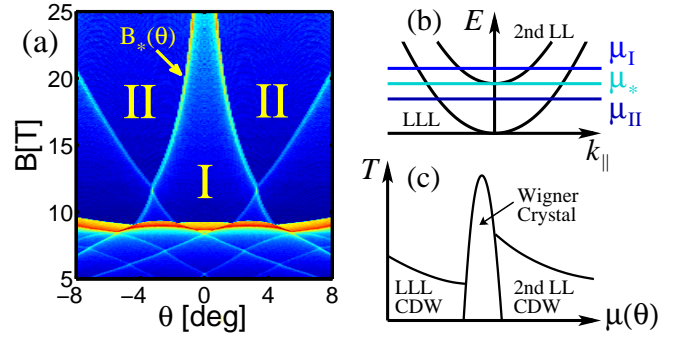


FIG. 1: (a) Single-particle DOS, excluding the contribution from the electron pocket invisible in torque experiments [5]. All electron pockets occupy the 2nd LL in region I, while pocket 3 empties into the LLL in region II. (b) Schematic energy dispersion for pocket 3 and (c) proposed phase diagram with interactions near  $B_*(\theta)$ .

emptying its 2nd LL. To address this aspect of experiment, we study interaction effects near this band emptying, employing Functional Renormalization Group (FRG) techniques similar to Ref. 8 and going beyond the early analysis of Abrikosov [9]. As the Fermi energy passes from above the 2nd LL into the LLL, we find that the leading instability for these electrons involves charge-density-wave (CDW) order in the 2nd LL, followed by Wigner crystal formation and LLL CDW order [see Fig. 1(c)]. We suggest that the hysteresis originates from the Wigner crystal phase, and discuss experiments to verify this proposal. Finally, we comment briefly on the Nernst and Hall effect puzzles, which remain unexplained by this work.

*Low-energy theory.* Our starting point is the tight-binding model of Liu and Allen [10], which was constructed to accurately reproduce bismuth’s band structure near the Fermi level [1]. We derive from this microscopic model an effective low-energy Hamiltonian for the electrons and holes in a magnetic field  $\mathbf{B}$  by expanding the lattice fermion operators as follows,

$$f_{\mu j \alpha}(\mathbf{r}) \sim e^{i\mathbf{Q}\cdot\mathbf{r}} \varphi_{\mu j \alpha}^{\beta} h_{\beta}^{\dagger} + \sum_{\lambda=1}^3 e^{i\mathbf{P}_{\lambda}\cdot\mathbf{r}} \sum_{\ell=1}^4 \phi_{\mu j \alpha}^{\lambda \ell} \psi_{\lambda \ell}, \quad (1)$$

where  $\mu = s, p_{x,y,z}$  labels the outer-shell orbital with spin  $\alpha = \uparrow / \downarrow$  at site  $\mathbf{r}$  on sublattice  $j = 1, 2$ . The two-component operators  $h$  describe hole excitations near wavevector  $\mathbf{Q}$  and the four-component Dirac fermions  $\psi_\lambda$  describe electron excitations near  $\mathbf{P}_\lambda$ ; the corresponding wavefunctions are  $\varphi^\beta$  and  $\phi^{\lambda\ell}$ . Using Eq. (1), we obtain the non-interacting Hamiltonian  $H_0 = \int_{\mathbf{r}} (h^\dagger \mathcal{H}_h h + \sum_\lambda \psi_\lambda^\dagger \mathcal{H}_e^\lambda \psi_\lambda)$ ,

$$\mathcal{H}_h = -\mu_h - \frac{D_x^2 + D_y^2}{2m_\perp} - \frac{D_z^2}{2m_z} - \frac{g_h \mu_B B^z \sigma^z}{2} \quad (2)$$

$$\mathcal{H}_e^3 = -\mu_e + m\mu^z - i \sum_{j=x,y,z} v_j D_j \eta^j - \frac{\mu_B \mathbf{G} \cdot \mathbf{B}}{2}. \quad (3)$$

Here  $\mathbf{D} = \nabla - iq\mathbf{A}$ , with  $\mathbf{B} = \nabla \times \mathbf{A}$  and  $q = \pm e$  for the holes and electrons, respectively. We employ three sets of Pauli matrices  $\sigma^j$ ,  $\tau^j$ , and  $\mu^j$  above, and define  $\eta^x = \mu^x (v_{1x}\tau^y + v_{2x}\tau^z)/v_x$  and  $\eta^{y,z} = (v_{1y,z}\mu^y + v_{2y,z}\tau^x\mu^x)/v_{y,z}$ , where  $v_{1j}^2 + v_{2j}^2 = v_j^2$ . The Hamiltonians  $\mathcal{H}_e^{1,2}$  for pockets 1 and 2 can be obtained from  $\mathcal{H}_e^3$  by rotating  $\mathbf{D}, \mathbf{B}$  by  $\pm 2\pi/3$  about the trigonal ( $z$ ) axis. In terms of the electron mass  $m_e$  and speed of light  $c$ , we have  $\mu_e = 0.0335\text{eV}$ ,  $\mu_h = 0.012\text{eV}$ ,  $m_\perp = 0.0675m_e$ ,  $m_z = 0.612m_e$ ,  $m = 6\text{meV}$ ,  $v_{1x} = 0.0022c$ ,  $v_{2x} = -0.002c$ ,  $v_{1y} = -7.6 \times 10^{-5}c$ ,  $v_{2y} = 3.4 \times 10^{-4}c$ ,  $v_{1z} = 0.002c$ ,  $v_{2z} = -0.0014c$ . The Fermi energy  $E_F = 0$  when  $\mathbf{B} = \mathbf{0}$ , but changes to maintain charge neutrality when  $\mathbf{B} \neq \mathbf{0}$ .

Zeeman coupling warrants further discussion. Microscopically, Zeeman energy has one source  $\propto \mathbf{B} \cdot (\mathbf{L} + 2\mathbf{S})$  and another coming from spin-orbit coupling  $\propto (\nabla U \times \mathbf{A}) \cdot \mathbf{S}$ , where  $U$  is the crystal potential and  $\mathbf{L}, \mathbf{S}$  denote orbital/spin angular momentum. While the corresponding low-energy terms can be obtained via Eq. (1), evaluating the spin-orbit contribution is nontrivial since the potential  $U$  is unknown. Progress can be made, however, by assuming  $U$  is rotationally invariant, as then only two independent matrix elements remain:  $\chi_{s/p} = \frac{1}{4m_e c^2} \langle s/p_x \uparrow | r \partial_r U \sin^2 \theta | s/p_x \uparrow \rangle$ , where  $|s/p_x \uparrow \rangle$  are the atomic  $s/p_x$  orbital wavefunctions. With this assumption, we obtain the hole Zeeman splitting in Eq. (2), which is sensitive only to  $B^z$ , consistent with experiment [4]. For the electrons, we obtain the Zeeman coupling in Eq. (3) with  $G_x = \tau^x (g_{1x} + g_{2x}\mu^z)$  and  $G_{y,z} = \tau^y (g_{1y,z} + g_{2y,z}\mu^z) + \tau^z (g_{3y,z} + g_{4y,z}\mu^z)$ . The  $g$ -factors are listed in Table I. Crucially,  $g_h$  depends only on  $\chi_p$ , and the electron  $g$ -factors obtain only a weak contribution from  $\chi_s$  because the wavefunctions  $\phi^{\lambda\ell}$  are concentrated on the  $p$ -orbitals. The precise value of  $\chi_s$  is therefore unimportant, and we will simply set  $\chi_s = \chi_p$ . Finally, hole Zeeman splitting has been well-studied experimentally [11], and from the available data we deduce that  $g_h \approx 54$ , which allows us to determine  $\chi_p$  and hence the electron  $g$ -factors.[17]

Equations (2) and (3) constitute the first major result of this paper. Most importantly, the electron Zeeman coupling has not been considered previously, and modifies the spectrum dramatically at high fields as we now discuss.

*Single-particle spectrum.* While the hole Hamiltonian is easily diagonalized, the electron part is much more difficult

	$a$	$b$	$c$		$a$	$b$	$c$
$g_h$	4	2	0	$g_{4y}$	-0.097	-0.35	-0.069
$g_{1x}$	1.5	1.3	0.072	$g_{1z}$	0.32	0.18	-0.024
$g_{2x}$	-1.4	-0.44	-0.024	$g_{2z}$	0.68	0.38	0.07
$g_{1y}$	-1.5	-0.9	-0.019	$g_{3z}$	-0.18	-0.42	-0.019
$g_{2y}$	-1.3	-0.76	0.0037	$g_{4z}$	-0.017	0.26	0.0038
$g_{3y}$	0.17	0.39	0.023				

TABLE I: Electron/hole  $g$ -factors, with  $g_\alpha = a_\alpha + b_\alpha \chi_p + c_\alpha \chi_s$ .

since the Zeeman and orbital terms do not commute. Qualitatively, Zeeman coupling generates components of higher LLs in the wavefunctions compared to the orbital-only problem and splits the usual LL degeneracy in the Dirac spectrum (see, e.g., Supporting Online Material for Ref. 5). To proceed, we truncate the Hilbert space, including only the first  $n \sim 10$  LLs, and diagonalize the Hamiltonian numerically.

Motivated by magnetization experiments [5], we have studied the spectrum for fields tilted by an angle  $\theta$  from the trigonal towards the binary axis. Figure 1(a) displays the single-particle density of states (DOS) in the  $B - \theta$  plane (excluding the electron pocket invisible to experiments [5]). Bright lines occur where the Fermi energy crosses the bottom of a LL, and the flat line at  $\sim 9\text{T}$  corresponds to the hole quantum limit. Remarkably, the electrons give rise to features at much higher fields which agree well with the anomalous structure reported experimentally (see Fig. 3 in Ref. 5).

The persistence of this structure up to such large fields arises from an increase in carrier density with field [4] and the splitting of the electron LL degeneracy by Zeeman coupling, which makes 2nd LL states available at lower energies and strongly suppresses the electron quantum limit. Indeed, in region I of Fig. 1(a) all electron pockets occupy the 2nd LL. Tilting the field into region II pushes one of those pockets (assumed to be pocket 3 hereafter) into the LLL. The dispersion for pocket 3 versus the momentum  $k_\parallel$  along the field appears schematically in Fig. 1(b), together with the chemical potential in I and II. Interestingly, experiments observed hysteresis in the magnetization at the line labeled  $B_*(\theta)$  separating these regions [corresponding to  $\mu_*$  in Fig. 1(b)]. Addressing this puzzle requires moving beyond single-particle physics.

*Correlation effects.* We now add Coulomb interactions,

$$H_{\text{int}} = \frac{1}{2} \int_{\mathbf{r}\mathbf{r}'} V(\mathbf{r} - \mathbf{r}') \rho(\mathbf{r}) \rho(\mathbf{r}'), \quad (4)$$

where  $\rho = \sum_\lambda \psi_\lambda^\dagger \psi_\lambda - h^\dagger h$  and  $V(\mathbf{r})$  is the screened Coulomb potential. Note that the number of holes and electrons within each pocket remains separately conserved here. Short-range pieces arising from lattice effects break this symmetry, but are subdominant and can be neglected.

Interactions can be most simply treated at weak coupling, which is controlled provided the dimensionless interaction strengths satisfy  $e^2/v_a^n \ll 1$ , where  $v_a^n$  is the Fermi velocity for pocket  $a$  in LL  $n$ . This criterion inevitably breaks down near a band emptying since at least one  $v_a^n \rightarrow 0$ . Correla-

tion effects will be most pronounced in this strongly coupled regime, and this is indeed where hysteresis appears. Our aim now is to study the crossover from weak to strong coupling to understand this aspect of experiment. Rather than addressing the fate of all carriers, we will focus more narrowly on the *leading* instability involving pocket 3 electrons near  $B_*(\theta)$ .

Even this restricted question requires considering numerous interactions, since  $H_{\text{int}}$  couples pocket 3 to all other carriers, some of which occupy more than one LL. We can, however, further distill the problem using an intuitive principle: similar carriers generally couple more effectively than dissimilar ones. For instance, velocity anisotropies sharply distort the electron LL wavefunctions, which strongly suppresses instabilities involving *different* electron pockets.[18] Furthermore, the hole and electron Fermi velocities differ significantly, which disfavors electron-hole pairing. We will therefore concentrate on interactions involving *only* pocket 3 electrons, commenting briefly on other couplings. For the three important cases [regions I, II, and the line  $B_*(\theta)$ ], we employ the FRG method to determine the leading instability. FRG equations give the renormalized interactions at length scale  $L$  as a function of the logarithmic rescaling factor  $\ell = \ln(L/\lambda)$ , where  $\lambda$  is a microscopic length of order the Fermi wavelength.

We begin in region II, where pocket 3 is confined to the LLL. To obtain a low-energy Hamiltonian we linearize the kinetic energy around the Fermi momenta  $\pm k_{F3}^0$ , expand  $\psi_3$  in terms of right/left movers, and project onto the LLL (we employ Landau gauge and label the transverse momentum  $k_{\perp}$ ). Interactions between pocket 3 electrons can then be written

$$H_{\text{int}}^{3,\text{II}} = \int_{\mathbf{k}_i} \rho(k_{\perp 1}, k_{\perp 2}) c_{R3}^{0\dagger}(\mathbf{k}_1 + \mathbf{k}_3) c_{L3}^{0\dagger}(\mathbf{k}_2 + \mathbf{k}_3) \times c_{L3}^0(\mathbf{k}_3) c_{R3}^0(\mathbf{k}_1 + \mathbf{k}_2 + \mathbf{k}_3), \quad (5)$$

where  $\mathbf{k} = (k_{\perp}, k_{\parallel})$  and  $c_{R/L3}^{0\dagger}$  creates a right/left-moving LLL electron. The FRG equation for the coupling function  $\rho(k, x) \equiv \rho(\mathbf{r})$  Fourier transformed in the second argument is

$$\partial_{\ell} \rho(\mathbf{r}) = \frac{1}{2\pi v_3^0} [\rho(\mathbf{r})^2 - (\rho * \rho)(\mathbf{r})], \quad (6)$$

with  $(f * g)(\mathbf{r}) = \int_{\mathbf{r}', \mathbf{r}''} e^{i(\mathbf{r}' \wedge \mathbf{r}' + \mathbf{r}' \wedge \mathbf{r}'' + \mathbf{r}'' \wedge \mathbf{r})} f(\mathbf{r}') g(\mathbf{r}'')$ . The solution to Eq. (6) is well-understood [8, 12]. The first term in the  $\beta$  function causes  $\rho$  to flow off, driving condensation of  $\langle c_{3R}^{0\dagger} c_{3L}^0 \rangle$  which gaps this channel and yields  $2k_{F3}^0$  CDW order along the field; the second term merely reduces the transition temperature [8]. Furthermore, it follows from the initial conditions that  $\rho(\mathbf{r} = \mathbf{0})$  is largest at the instability, so that the transverse density is uniform in the CDW phase. As an aside, we note that coupling to other electron pockets and the holes leads to a series of couplings with flow equations analogous to Eq. (6). Due to the velocity anisotropy discussed above, inter-pocket electron instabilities set in at very low energies, and are preempted by the  $\rho$  instability. Similarly, since the hole velocity is several times smaller than  $v_3^0$ , hole-hole pairing preempts the ‘excitonic’ instability [13] in the electron-hole channel.

Next, we sit at  $B_*(\theta)$  and fine-tune the chemical potential to  $\mu_*$  in Fig. 1(b), precisely at the bottom of the 2nd LL. At low energies, we now have linearly-dispersing right/left movers  $c_{R/L3}^0$  coupled with *quadratically* dispersing 2nd LL electrons which we denote by  $d_3^1$ . As it stands, the problem can not be treated within weak coupling since the soft dispersion for the latter renders interactions involving  $d_3^1$  strongly relevant at the non-interacting fixed point. To proceed, we follow Ref. 14 and seek a controlled limit by replacing the 2nd LL kinetic energy  $Dk_{\parallel}^2$  with  $D|k_{\parallel}|^{1+\epsilon}$  and performing an expansion in  $\epsilon$  and the interaction strength in the limit  $1 \gg \epsilon \sim e^2/v_3^0$ .

Pocket 3 interactions now involve several couplings:

$$H_{\text{int}}^{3,B_*} = \int_{\mathbf{k}_i} \{ \rho(k_{\perp 1}, k_{\perp 2}) c_{3R}^{0\dagger}(\mathbf{k}_1 + \mathbf{k}_3) c_{L3}^{0\dagger}(\mathbf{k}_2 + \mathbf{k}_3) \times c_{L3}^0(\mathbf{k}_3) c_{R3}^0(\mathbf{k}_1 + \mathbf{k}_2 + \mathbf{k}_3) + u d_3^{1\dagger} d_3^1 d_3^1 d_3^1 \quad (7) \\ + [v c_{3R}^{0\dagger} d_3^1 d_3^1 c_{R3}^0 + (R \rightarrow L)] + [w c_{3R}^{0\dagger} c_{3L}^{0\dagger} d_3^1 d_3^1 + h.c.] \}.$$

The arguments in the last three couplings have been suppressed for brevity, but should appear as in the  $\rho$  term. Fourier transforming in the second argument and defining  $\mathbf{r} = (k, x)$  as before, it will be convenient below to write the flow equations for these coupling functions as follows:

$$\begin{aligned} \partial_{\ell} \rho(\mathbf{r}) &= \frac{1}{2\pi v_3^0} [\rho(\mathbf{r})^2 - (\rho * \rho)(\mathbf{r})] - \frac{\alpha}{\pi} (w * w^*)(\mathbf{r}), \\ \partial_{\ell} u(\mathbf{r}) &= \epsilon u(\mathbf{r}) + \frac{\beta}{\pi} u(\mathbf{r})^2 - \frac{\alpha}{\pi} (u * u)(\mathbf{r}) \\ &\quad - \frac{1}{2\pi v_3^0} (w^* * w)(\mathbf{r}), \quad (8) \\ \partial_{\ell} v(\mathbf{r}) &= \frac{\gamma_1}{2\pi} [v(\mathbf{r})^2 - (v * v)(\mathbf{r})] + \frac{2\gamma_2}{\pi} |w(\mathbf{r})|^2, \\ \partial_{\ell} w(\mathbf{r}) &= \frac{\epsilon}{2} w(\mathbf{r}) - \frac{1}{2\pi v_3^0} (\rho * w)(\mathbf{r}) - \frac{\alpha}{\pi} (w * u)(\mathbf{r}) \\ &\quad + \frac{\gamma_1}{\pi} v(\mathbf{r}) w(\mathbf{r}) - \frac{\delta}{\pi} \int_{\mathbf{r}'} e^{i\mathbf{r} \wedge \mathbf{r}'} v(\mathbf{r}') w(\mathbf{r}'). \end{aligned}$$

Here  $\alpha = 1/D$ ,  $\gamma_1 = \delta = 1/(v_3^0 + D\lambda^{\epsilon} e^{-\epsilon\ell})$ ,  $\gamma_2 = \gamma_1 \lambda^{\epsilon} e^{-\epsilon\ell}$ , and  $\beta = 0$ . Naively, power-counting suggests that  $u$  flows off first. However, since  $\beta = 0$ , the analogous term that drove the CDW instability in region II is absent, which leaves open a more interesting possibility.

To facilitate analytic and numeric progress, we now approximate  $V(\mathbf{r})$  as local (anisotropies can then be scaled away). Note first that at the initial conditions,  $w$  is suppressed compared to  $\rho, u, v$  since terms that survive Pauli exclusion are suppressed due to small overlaps between the participating LL wavefunctions. Thus we begin by setting  $w = 0$ , which decouples the remaining equations. Clearly both  $\rho$  and  $v$  then flow off, with the former diverging faster since  $\rho$  is larger at the initial conditions. The behavior of  $u$  is less obvious. Assuming  $u(k, x)$  is rotationally invariant (after rescaling) and analytic in  $k, x$ , we can solve the flows for  $u$  by assuming an ansatz  $u(\mathbf{r}; \ell) = \sum_j f_j(\ell) \chi_j(r)$ . Here  $j$  runs over 0, 2, 4, ... and  $\chi_j(r) = e^{-r^2/2} P_j(r)$ , with  $P_j(r)$  degree- $j$  polynomials

defined so that  $(\chi_j * \chi_{j'})(\mathbf{r}) = \delta_{j,j'} C_j \chi_j(r)$ . One then obtains decoupled equations for each  $f_j$  which show that  $u(\mathbf{r}; \ell)$  flows to a finite fixed point provided  $C_j f_j(0) \geq 0$  for all  $j$ . In our problem the initial conditions are well-approximated by  $u(\mathbf{r}; \ell = 0) = c(r^2 - 1)e^{-r^2/2} \propto \chi_2(r)$ , with  $c > 0$ , which indeed remains finite under renormalization. Though this result is correct in the  $\epsilon$ -expansion, we caution that the fixed point *could* move to strong coupling for physical  $\epsilon = 1$ . This would imply a  $u$ -driven instability (see below).

To treat the full problem with  $w \neq 0$  we rely on numerical integration of the FRG equations. Here we find that  $w$  further enhances the instability in  $\rho$ , and also generates additional non-zero components of  $\chi_j$  in  $u$ , causing this function to flow off in tandem with  $w$ . In contrast,  $v$  is only weakly affected by  $w$  and remains unimportant. Because  $\rho$  was already unstable when  $w = 0$ , this function becomes of order one first, driving CDW order in the LLL with uniform transverse density. The leading instability in the 2nd LL occurs soon after driven by  $u$ , which localizes these states producing Wigner crystallization as the chemical potential increases. While this is certainly reasonable, we caution that definitively ruling out the scenario where  $u$  provides the leading instability is difficult due numerical limitations, particularly when  $V(\mathbf{r})$  is non-local. In this case the order of the instabilities is simply reversed.

Finally, consider region I, with the chemical potential slightly above the 2nd LL for pocket 3. This problem is reminiscent of a 1D wire with 2 transverse modes occupied [15], though the LLs change the physics qualitatively. As in region II, we derive a low-energy theory for right/left movers in the LLL,  $c_{3R/L}^0$ , and 2nd LL,  $c_{3R/L}^1$ . Interactions then read

$$H_{\text{int}}^{3,I} = \int_{\mathbf{k}_i} \{ \rho(k_{\perp 1}, k_{\perp 2}) c_{3R}^{0\dagger}(\mathbf{k}_1 + \mathbf{k}_3) c_{L3}^{0\dagger}(\mathbf{k}_2 + \mathbf{k}_3) \\ \times c_{L3}^0(\mathbf{k}_3) c_{R3}^0(\mathbf{k}_1 + \mathbf{k}_2 + \mathbf{k}_3) + u c_{3R}^{1\dagger} c_{3L}^{1\dagger} c_{3L}^1 c_{3R}^1 \quad (9) \\ + [v c_{3R}^{0\dagger} c_{3L}^{1\dagger} c_{3L}^0 c_{R3}^0 + (R \rightarrow L)] + [w c_{3R}^{0\dagger} c_{3L}^{0\dagger} c_{3L}^1 c_{3R}^1 + h.c.] \},$$

where again the arguments of the last three couplings should appear as in the first. These couplings flow as in Eqs. (8), but with  $\epsilon = \delta = 0$ ,  $\alpha = \beta = 1/(2v_3^1)$ , and  $\gamma_1 = 4\gamma_2 = 2/(v_3^0 + v_3^1)$ . It is natural to suspect here that  $u$  dominates, since the 2nd LL carriers have the slowest velocity. This is indeed correct, which can be understood analytically by ignoring all  $(f * g)$  terms in Eqs. (8). Since  $\beta$  is the largest coefficient remaining when the 2nd LL is weakly populated,  $u$  flows off before all other couplings, driving CDW order formed by condensing  $\langle c_{3R}^{1\dagger} c_{3L}^1 \rangle$ . The transverse density becomes Wigner crystalline [12] at the instability, since the form of the 2nd LL Dirac wavefunctions dictates that  $u(\mathbf{r})$  is maximized at  $\mathbf{r} \neq 0$ . In the limit where  $V(\mathbf{r})$  is local, we have verified numerically that terms neglected in this crude analysis do not modify these conclusions.

*Discussion.* Putting our results together, we propose the minimal phase diagram shown in Fig. 1(c). We speculate that experiments of Ref. 5 may be conducted above the critical temperature for the CDW phases in regions I and II but below

that for the Wigner crystal phase near the boundary. The latter transitions are almost certainly first order, which would be consistent with the observed hysteresis. However, *two* transitions ought to occur here, whereas experiments see only one. This issue can be resolved by invoking disorder, which will be particularly important in the low-density region of the Wigner crystal phase close to region II. The transition on that side is expected to be smeared by disorder-pinning of the localized states, which should be addressed in more detail. Future experiments, particularly nonlinear transport and x-ray scattering studies to search for signs of CDW and Wigner crystal order, should provide valuable clues as to the true nature of this transition.

The Hall and Nernst effect puzzles in trigonal fields  $B > 9\text{T}$  [6] are difficult to resolve at weak coupling. Here hole-hole pairing drives the leading CDW instability, which is not expected to recover these anomalies. While surface states should be seriously considered as emphasized in Ref. 5, we believe a more exotic origin is not inconceivable. Interactions between the LLL holes are *not* weak, as  $e^2/v_h^0 \sim 24$ , well outside of the range where weak coupling is expected to be reliable. In contrast, interactions between LLL electrons, while not necessarily weak, are several times smaller:  $e^2/v_e^0 \sim 5$ . Although screening should reduce these somewhat, the problem warrants studying from a strong-coupling standpoint, which presents an exciting research direction [16].

It is a pleasure to acknowledge illuminating discussions with K. Behnia, Lu Li, O. Motrunich, N.P. Ong, and G. Refael, as well as the hospitality of the KITP where this work was initiated. We also acknowledge support from the Lee A. DuBridge Foundation (JA), and the Packard Foundation and National Science Foundation through grants DMR-0804564 and PHY05-51164 (LB).

- 
- [1] V. S. Edel'man, *Adv. Phys.* **25**, 555 (1976).
  - [2] L. Fu and C. L. Kane, *Phys. Rev. B* **76**, 045302 (2007).
  - [3] D. Hsieh *et al.*, *Nature* **452**, 970 (2008).
  - [4] G. E. Smith *et al.*, *Phys. Rev.* **135**, A1118 (1964).
  - [5] L. Li *et al.*, *Science* **321**, 547 (2008).
  - [6] K. Behnia *et al.*, *Science* **317**, 1729 (2007).
  - [7] M. H. Cohen and E. I. Blount, *Phil. Mag.* **5**, 115 (1960).
  - [8] V. M. Yakovenko, *Phys. Rev. B* **47**, 8851 (1993).
  - [9] A. A. Abrikosov, *J. Low Temp. Phys.* **10**, 3 (1973).
  - [10] Y. Liu and R. E. Allen, *Phys. Rev. B* **52**, 1566 (1995).
  - [11] S. G. Bompadre *et al.*, *Phys. Rev. B* **64**, 073103 (2001).
  - [12] S.-W. Tsai *et al.*, *Phys. Rev. B* **65**, 241102 (2002).
  - [13] B. I. Halperin and T. M. Rice, *Rev. Mod. Phys.* **40**, 755 (1968).
  - [14] L. Balents and M. P. A. Fisher, *Phys. Rev. B* **53**, 12133 (1996).
  - [15] J. S. Meyer *et al.*, *Phys. Rev. Lett.* **98**, 126404 (2007).
  - [16] F. J. Burnell *et al.*, arXiv:0810.1757 (unpublished).
  - [17] The data of Ref. 11 appear consistent with the hole Zeeman splitting being  $2 \pm 0.16$  times the cyclotron energy. We use the lower sign, which gives  $g_h = 54$ , since the hole quantum limit then occurs closer to 9T as observed experimentally.
  - [18] Fields oriented so that 2 or 3 pockets are symmetry-related may produce instabilities involving multiple electron pockets.